

Flow through three-dimensional self-affine fractures

H. J. Seybold,^{1,2} H. A. Carmona,¹ F. A. Leandro Filho,¹ A. D. Araújo,¹ F. Nepomuceno Filho,¹ and J. S. Andrade Jr.^{1,*}

¹*Departamento de Física, Universidade Federal do Ceará,
Campus do Pici, 60451-970 Fortaleza, Ceará, Brazil*

²*Physics of Environmental Systems, D-USYS, ETH, Zurich, 8093 Zurich, Switzerland*

We investigate through numerical simulations of the Navier-Stokes equations the influence of the surface roughness on the fluid flow through fracture joints. Using the Hurst exponent H to characterize the roughness of the self-affine surfaces that constitute the fracture, our analysis reveals the important interplay between geometry and inertia on the flow. Precisely, for low values of Reynolds numbers Re , we use Darcy's law to quantify the hydraulic resistance G of the fracture and show that its dependence on H can be explained in terms of a simple geometrical model for the tortuosity τ of the channel. At sufficiently high values of Re , when inertial effects become relevant, our results reveal that nonlinear corrections up to third-order to Darcy's law are approximately proportional to H . These results imply that the resistance G to the flow follows a universal behavior by simply rescaling it in terms of the fracture resistivity and using an effective Reynolds number, namely, Re/H . Our results also reveal the presence of quasi-one-dimensional channeling, even considering the absence of shear displacement between upper and lower surfaces of the self-affine fracture.

I. INTRODUCTION

Understanding the behavior of a fluid flowing through a fractured rock is of great importance in many practical applications [1–5]. In particular, it is crucial to investigate how the fracture's surface morphology influences the flow resistance in driving fluids through naturally or artificially fractured carbonate reservoirs [6–9]. Since at the reservoir scale fractures are mostly composed of networks of interconnected cracks with very different sizes, it is important to understand how the behavior of the flow in a single fracture scales with its size, as well as how it is affected by the details of its geometry [7]. The local flow structures are a direct result of the fracture's morphology and many studies have been devoted to understand their upscale in order to derive consistent macroscopic relations [10–13].

It is generally accepted that the morphology of brittle fractures follows *self-affine* scaling laws [14]. More precisely, it means that by re-scaling an in-plane vector \mathbf{r} by $\lambda\mathbf{r}$, the out-of-plane coordinate z needs to be re-scaled by $\lambda^H z$ for the surface to remain statistically invariant, where the scaling exponent H is called the Hurst exponent. It was first suggested that rock fractures have a unique exponent $H = 0.8$ [15–21]. However, recent studies indicate that some natural fractured systems exhibit other values of H (ranging from 0.45 to 0.85) depending on the material and the fracturing process [22–25]. As a result, more than one universality class exists for fractured rocks and therefore it is important to understand how the flow properties are affected by variations in the Hurst exponent.

A single-phase flow in a fractured rock is usually characterized in terms of Darcy's law [3, 26, 27], which defines a linear relation between the mean flow velocity U and the pressure drop ΔP across the system, namely $U = -k\Delta P/\mu L$. Here μ is the fluid's viscosity, L is the length of the fracture in the flow direction, and the proportionality constant k is the permeability. Essentially Darcy's law is a good approximation at low Reynolds numbers, $Re = \rho U w/\mu \ll 1$, where w is usually taken as the aperture of the fracture and ρ is the density of the fluid. However, in order to understand the interplay between the geometry and the flow inside the fracture, it is necessary to examine *local* aspects of the surface roughness and relate them to the relevant mechanisms of momentum transfer through viscous and inertial forces.

The influence of surface roughness on the flow properties inside a fracture has been first studied theoretically by Roux *et al.* [10]. They predicted that the permeability of a self-affine fracture should scale with the length of the system as $k \sim L^{2H}$. This result is based on the assumption that the fracture behaves like a system of parallel plates with an effective aperture w , where the self-affinity implies that $w \sim L^H$, and $k \sim w^2$ follows the solution of the Stokes equation. Since then, several theoretical and experimental studies focused on how the permeability scales with the fracture's opening and length in the viscous flow regime. Using perturbation theory, Drazer and Koplik [28] calculated for two-dimensional flows that the permeability should scale as $k_0 - k \sim L^H$, where k_0 is the permeability of the unperturbed system. Later they extended their study to three-dimensional flows and confirmed these results in terms

* soares@fisica.ufc.br

of the effective medium analysis and numerical simulations at low Reynolds numbers. Talon *et al.* [11] conjectured that the permeability is controlled by the minimum aperture of the fracture w_{min} and found that, for two-dimensional flows, $k \propto w_{min}^{3-1/H}$. For three-dimensional flows, however, Talon *et al.* have shown numerically that $k \sim w_{min}^{2.25}$ for $H = 0.8$ and $k \sim w_{min}^{2.16}$ for $H = 0.3$.

The role of inertia on fluid flow through two-dimensional self-affine fractures has been addressed by Sketne *et al.* [29], who considered fractures with constant aperture and $H = 0.8$. Their numerical simulations show that, in the range of intermediate Reynolds number $Re \approx 1$, the flow can be described by a weak inertia equation [30, 31], whereas for moderate Reynolds numbers ($25 \leq Re \leq 52$) inertial effects can be described by the Forchheimer equation [32]. More recent numerical studies [33] extended these results for different Hurst exponents with long range correlations, namely $H > 0.65$.

It is evident that inertia has very different impact on two- and three-dimensional flow systems. Here we address the question on how the permeability and the nonlinear corrections to Darcy's law depend on the surface roughness of three-dimensional self-affine fractures. To do so we systematically examine the behavior of the fluids hydraulic resistance as a function of the Reynolds number in the range from $Re = 10^{-2}$ to $Re = 500$, and for different values of the Hurst exponent, varying from strongly anticorrelated $H = 0.3$ to strongly correlated values, $H = 0.9$.

The remainder of this paper is organized as follows. Section II describes the methodology we have used to generate the geometry, and the setup of the computer simulations. In Section III we present and discuss our simulation results and Section IV is devoted to the conclusions.

II. METHODS

The three-dimensional numerical domain used in our analysis consists of the volume between two identical self-affine surfaces, representing the fracture walls. The surfaces have been displaced perpendicular to the mean surface plane (the $x - y$ plane). Specifically, no additional shear displacement is added to the surfaces in this plane, so that the fracture aperture w is constant throughout the numerical domain (see Fig. 1).

The wall surfaces are generated using a two-dimensional generalization of the fractional Brownian Motion [34–37] which satisfies the following scaling relation:

$$\langle [z(\mathbf{r}_2) - z(\mathbf{r}_1)]^2 \rangle = \sigma_z^2 \left| \frac{\mathbf{r}_2 - \mathbf{r}_1}{L} \right|^{2H}, \quad (1)$$

where σ_z^2 is the mean square increment for points separated by a distance L . Here $z(\mathbf{r})$ defines the elevation of the wall surface and \mathbf{r} is a vector in the $x - y$ plane. The Hurst exponent H characterizes the spatial correlations of the surface. Surfaces with $H < 0.5$ are spatially anti-correlated, while for $H > 0.5$ long-range spatial correlations are present. For the case $H = 0.5$ we obtain ordinary Brownian surfaces formed by successive uncorrelated increments [37]. In order to create a discrete fractional Brownian surface with a given exponent H numerically, we use the Fourier filtering method [37, 38]. This method imposes a scaling behavior on the spectral density S_z as,

$$S_z(k) \propto \frac{1}{k^\xi}, \quad (2)$$

where the parameter ξ is related to the Hurst exponent via $\xi = 2 + 2H$ for two-dimensional surfaces [39]. Equation (2) is used to define the amplitudes of the discrete Fourier spectrum of the wall surface, which is then transformed back to real space using a fast Fourier transform.

For all fracture realizations, the aperture is kept constant, $w = 5$, and the length in x and y directions is set to be $L = 500$, both in dimensionless units. In order to obtain fractures with a comparable variability in the z -direction, the amplitude of the surfaces is also fixed for all realizations to be $\sigma_z = 5$ in dimensionless units.

We now turn our attention to the flow between the two rough fracture walls. The three-dimensional flow is described by the incompressible Navier-Stokes equations under isothermal steady-state conditions. The momentum and mass conservation equations are written as

$$\begin{aligned} \rho \mathbf{u} \cdot \nabla \mathbf{u} &= -\nabla p + \mu \nabla^2 \mathbf{u}, & (3) \\ \nabla \cdot \mathbf{u} &= 0, & (4) \end{aligned}$$

where \mathbf{u} , p and ρ are the velocity, pressure, and the fluid's density, respectively. We apply non-slip boundary conditions at the top and bottom walls. The fluid is injected in the x direction at $x = 0$ using a uniform velocity profile with amplitude U at the inlet, and a constant pressure defines the outlet boundary, at $x = L$. Laterally symmetrical boundary conditions were applied to minimize finite-size effects. In order to solve Eqs. (3) and (4) numerically, we

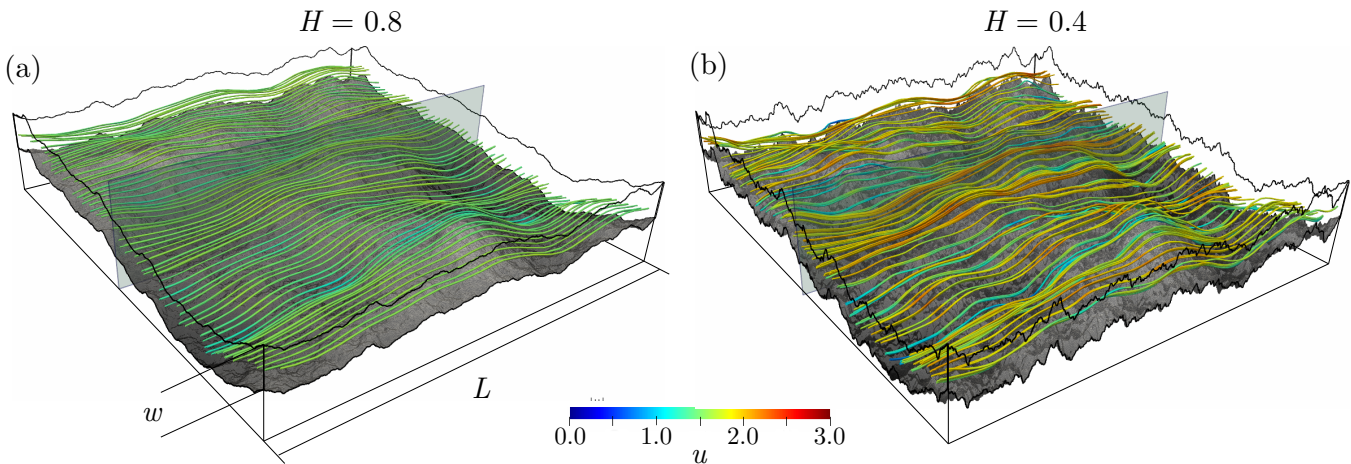


FIG. 1. Fluid flow through a typical fracture joint calculated for $\text{Re} = 100$ and Hurst exponents (a) $H = 0.8$ and (b) $H = 0.4$. The fluid flows from left to right. Streamlines are also shown, colored according to the local velocity magnitude.

first discretize the volume between the top and bottom surface of the fracture using a tree-dimensional unstructured hexahedral mesh generated using the OpenFOAM's meshing tool *snappyHexMesh* [40]. Close to the surface, the hexahedral cells were refined three times in order to capture small variations of the fracture surface.

For each value of the Hurst exponent in the range $0.3 \leq H \leq 0.9$, we generated five realizations of the computational domain to compute ensemble averages. For each realization, flow simulations are performed with different values of the Reynolds numbers in the range $0.01 \leq \text{Re} \leq 500$ by adjusting the inlet velocity U .

III. RESULTS AND DISCUSSION

The Forchheimer equation [32, 41] has been extensively used as an extension of Darcy's law to account for inertial corrections in flow through disordered pore structures [3, 27, 42]. Expectedly, the addition of higher-order corrections in the velocity to the Forchheimer equation allows for a better agreement with experimental data over the full range of the laminar regime [26, 43–45]. Up to cubic order, these corrections can be written as,

$$-\frac{\Delta P}{L} = \alpha \mu U + \beta \rho U^2 + \frac{\gamma \rho^2 U^3}{\mu}, \quad (5)$$

where $\alpha \equiv 1/\kappa$ corresponds to the reciprocal of the permeability of the channel, and β and γ are the coefficients of the second- and third-order corrections, respectively. Rewriting Eq.(5) in terms of Re , we obtain,

$$G = \alpha w^2 + \beta w \text{Re} + \gamma \text{Re}^2, \quad (6)$$

where $G \equiv -\Delta P w^2 / \mu U L$ is a dimensionless measure of the hydraulic *resistance* of the fracture. Figure 2 displays the results from all our numerical simulations, where G is plotted as a function of Reynolds number and for different values of the Hurst exponent. The solid lines are the nonlinear fits of Eq. (6) to the data sets in order to determine the coefficients α , β and γ .

For small Reynolds numbers, G is dominated by the viscous term in Eq. 6, namely, αw^2 , which decreases monotonically with the Hurst exponent H as shown in Fig. 3. Consistent with the results for a Poiseuille flow between two parallel planes with constant aperture w , it approaches the value $\alpha = 12/w^2$ for large values of H . In order to understand the particular form of this relation, we consider, as a first approximation, the fracture as composed of a sequence of parallel plates with varying angles with respect to the $x - y$ plane. For a self-affine fracture surface, one can define a *tortuosity* factor as,

$$\tau \equiv \frac{L_p}{L} = \sqrt{1 + \left(\frac{\sigma_z}{\delta x}\right)^2 \left(\frac{L}{\delta x}\right)^{-2H}}, \quad (7)$$

where L_p is the perimeter in the direction of the flow and $\delta x \ll L$ is the numerical resolution used to generate the rough surface (see Section I of the Supplemental Material). Considering this simplified geometrical model, we now

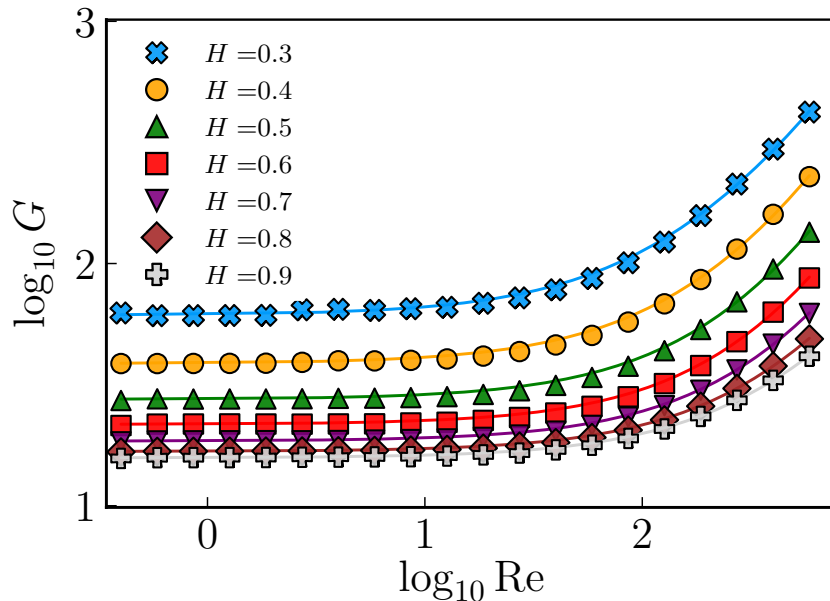


FIG. 2. Hydraulic resistance G as a function of the Reynolds number Re for different values of the Hurst exponent H . In all cases, the plateau corresponding to Darcy's law (constant G) is followed by a non-linear regime that reflects the effect of convection on the flow. The error bars are smaller than the symbols and the solid lines are the best fit to the data using Eq. (6). For each value of the parameters Re and H , the value of G is obtained as the average over a total of five realizations.

conjecture that the first term in Eq. (6) can be described as,

$$\alpha w^2 = a\tau + b. \quad (8)$$

Here, to be consistent with the limiting value for the hydraulic resistance of parallel plates at very low Re , the parameters a and b should be obtained from the numerical simulations with the constraint that $a+b = (\alpha w^2)_{min} \geq 12$. Figure 4 shows that αw^2 follows very closely Eq. (8) for $H \leq 0.7$. From the least-squares fit to the data, combining Eqs. (7) and (8) with $\sigma_z = 5$ and $\delta x = 2$, we obtain $a = -42.4 \pm 0.7$ and $b = 58.9 \pm 0.6$, which consistently gives $a + b = 16.5 \geq 12$. For large values of the Hurst exponent, the influence of the self-affine geometry on the flow is less strong because the local slopes in the channel are not so high as compared to those present in channels generated with smaller values of H . As a consequence, this purely geometrical model tends to overestimate the hydraulic resistance αw^2 for $H > 0.7$. This systematic discrepancy is better visualized in Fig. 3, where the solid black line is also obtained from Eqs. (7) and (8), with the same previously estimated parameters a and b .

In agreement with experiments [46], we observe that the transition from a linear (constant G) to a non-linear regime occurs at lower Re for rougher surfaces. Although the absolute value of G significantly depends on the tortuosity, and decreases with H , our results shown in Fig. 2 suggest that the general increasing trend of the nonlinear corrections as a function of Re is independent of the Hurst exponent. In order to quantify the impact of the surface roughness on the departure from Darcy's law, we plot G as a function of an effective Reynolds number, defined as Re/H . Following this procedure, all curves collapse onto a single master curve, as shown in Fig. 5. This collapse is an indication that the onset of the non-linear contributions to the hydraulic resistance increases in a linear fashion with the parameter H . As a matter of fact, the excellent quality of the collapse implies the scaling relations,

$$\beta w \propto \alpha w^2 / H \quad (9)$$

and

$$\gamma \propto \alpha w^2 / H^2. \quad (10)$$

As depicted in Fig. 6, the second-order term follows the proposed scaling relations rather well. For the third-order coefficient, however, we observe significant deviations from the proposed linear trend for $H < 0.4$ ($\alpha w^2 / H^2 > 110$).

Next, we analyze the impact of the surface roughness on the velocity field directly. Figures 1a and 1b show typical realizations of fluid flows through two fracture joints at $Re = 100$ for Hurst exponents $H = 0.4$ and 0.8 , respectively.

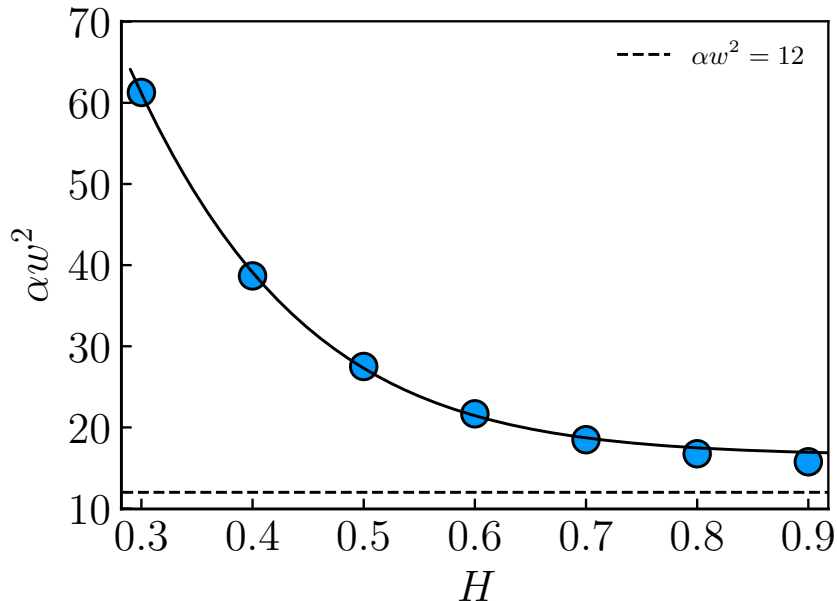


FIG. 3. Dependence of αw^2 on the Hurst exponent H . The parameter $\alpha \equiv 1/\kappa$ approaches the limiting value of $12/w^2$ (dashed black line), as expected for the Poiseuille flow. The solid black line is obtained by the combination of Eq. (8), with the previously estimated parameters a and b , and Eq. (7), with $\delta x = 2$, $\sigma_z = 5$ and $L = 500$.

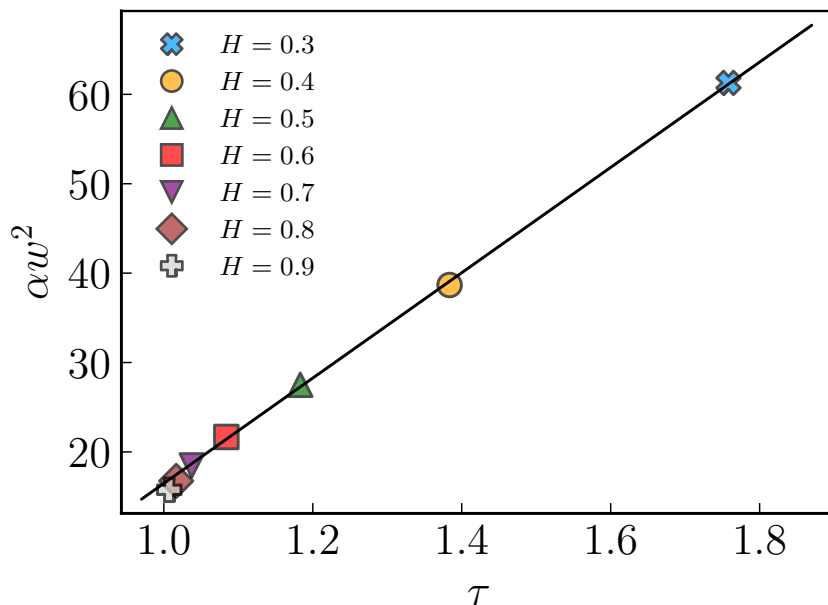


FIG. 4. Variation of αw^2 with the tortuosity τ . The error bars are smaller than the symbols. The solid lines correspond to the least-squares fit to the simulation data using $\alpha w^2 = a + b\tau$, with $a = -42.4 \pm 0.7$ and $b = 58.9 \pm 0.6$, where τ was computed from Eq. (7) with $\sigma_z = 5$ and $\delta = 2$.

Streamlines of the velocity field are also shown, being colored by the velocity magnitude. The contour plots in Fig. 7 denote the magnitude of the velocity field on the cross-sectional planes along the main flow direction, as indicated in Fig. 1. For the larger Hurst exponent, $H = 0.8$, the fluctuations in the local velocity field are visually smoother, with the maximum velocity near the center of the channel approximately equal to $3U/2$, as expected in the limiting case of parallel plates [47] (see Section II of the Supplemental Material). For $H = 0.4$, however, the situation is rather different. Due to continuity, regions of higher velocities are clearly more confined at the center of the channel, since

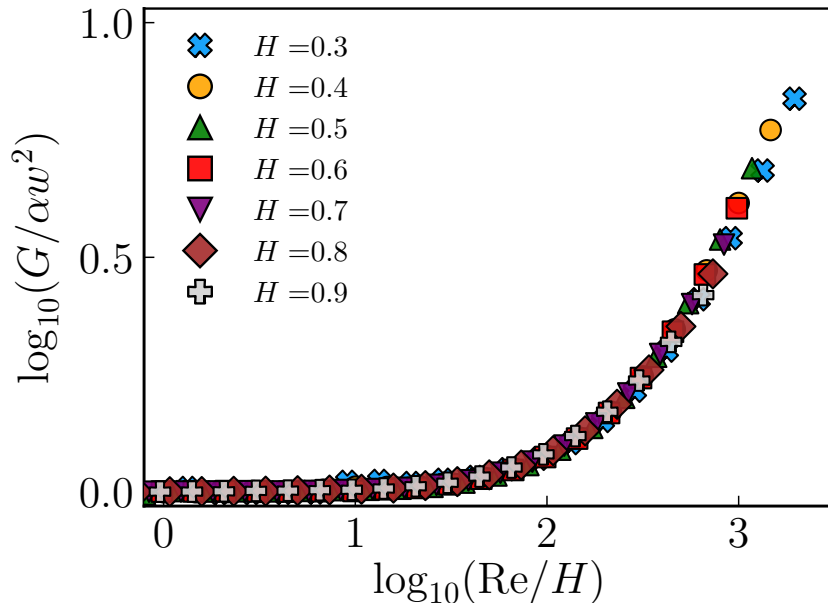


FIG. 5. Hydraulic resistance G as a function of Re/H . The excellent collapse of the simulation data onto a single curve indicates that the onset of the nonlinear contributions to the Darcy’s law increases linearly with the Hurst exponent.

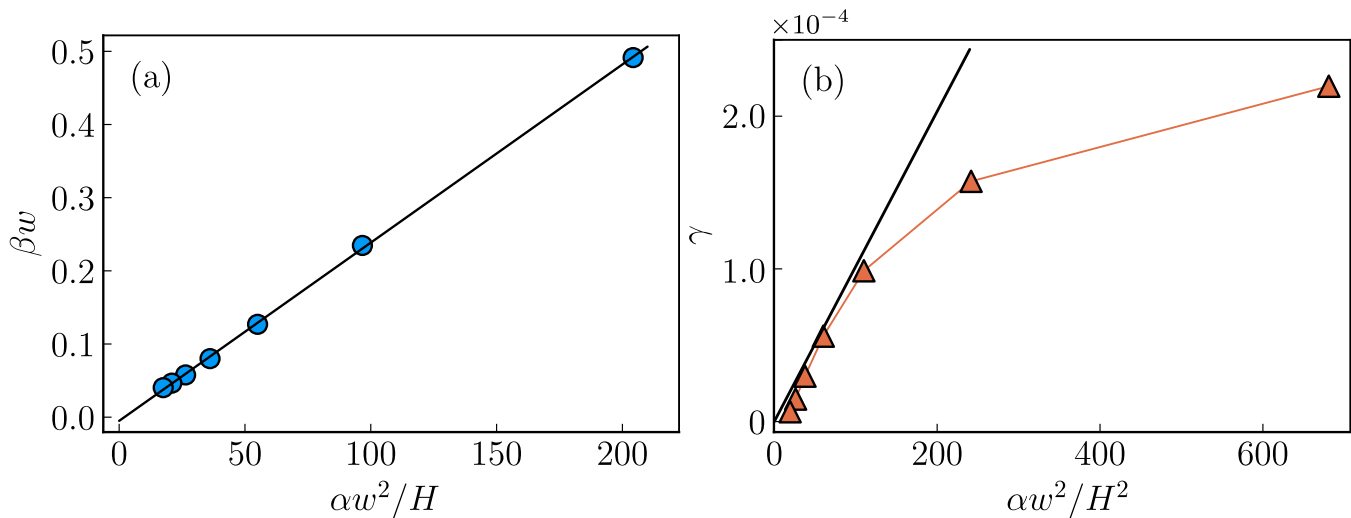


FIG. 6. (a) The parameter βw as a function of $\alpha w^2/H$. The black solid line corresponds to the least-squares fit to the data using $\beta w = c_0 (\alpha w^2/H)$ with $c_0 = 0.0023 \pm 0.0001$. (b) The scaling of γ with $\alpha w^2/H^2$. The solid line corresponds to $\gamma = c_1 (\alpha w^2/H^2)$ with $c_1 = (1.01 \pm 0.05) \times 10^{-6}$. The simulation data deviates from the expected linearity for small $H < 0.4$ ($\alpha w^2/H^2 > 110$).

the zones of almost stagnated flow close to walls broadens. As a consequence, the velocity magnitudes climb up to $2.5U$, which is consistent with a relatively higher effective Reynolds number, Re/H , as suggested by the collapse in Fig. 5. An enhancement in the velocity magnitude due to local disorder in the surface morphology can then persist and propagate further into the fracture joint forming preferential flow paths, where the fluid follows trajectories connecting “valleys” and around “mountains” of the rough surfaces. This effect is only possible in three-dimensional flows, since in two dimensions the flow is forced through local bottlenecks.

A similar preferential channeling effect has been found in previous experiments [48] and computational simulations [49–51]. This effect, however, has always been associated to an additional shear displacement between the upper and lower surface, which generates a heterogeneous aperture distribution throughout those fractures. Our simulations,

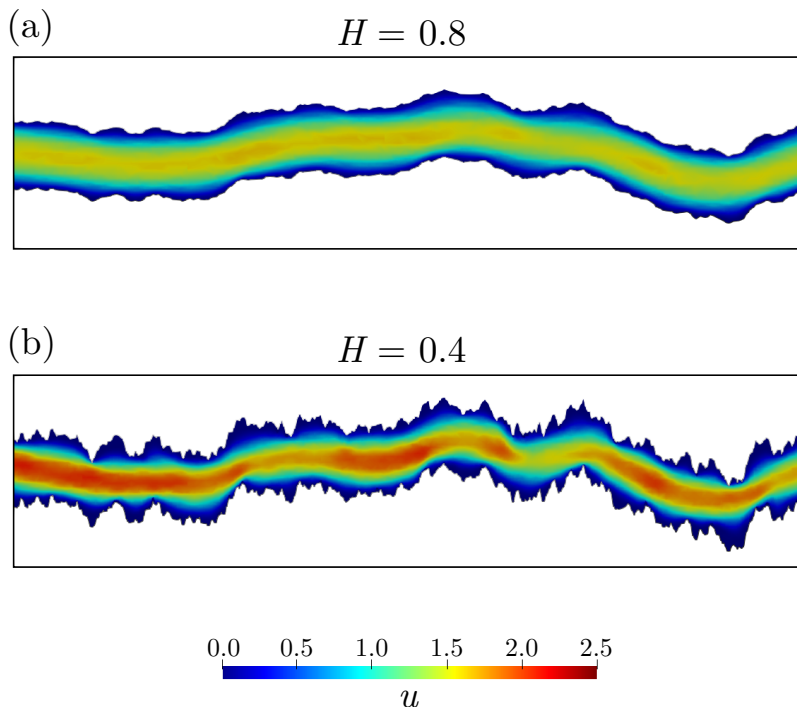


FIG. 7. Contour plots of the velocity magnitudes in the cross sections along the channels as indicated in Fig. 1, for $\text{Re} = 100$ and Hurst exponents (a) $H = 0.8$ and (b) $H = 0.4$.

however, show that no lateral displacement is needed and that the preferential channeling effect thus should be a result of an effective aperture field which is significantly affected by the surface topology.

The effect of preferential channeling can be quantified by the participation ratio π , which has been previously utilized to describe the spatial localization of kinetic energy inside the flow through disordered porous media [44], being defined as,

$$\pi = \frac{\langle e \rangle^2}{\langle e^2 \rangle}, \quad (11)$$

where $\langle e^n \rangle = (1/V) \iiint (\mathbf{u} \cdot \mathbf{u})^n d^3\mathbf{r}$ is the n^{th} moment of the kinetic energy and V is the volume of the system. If the kinetic energy is uniformly distributed across the sample, one obtains $\pi \rightarrow 1$, whereas if the flow field is strongly localized, $\pi \rightarrow 1/V$, approaching zero in the limit of an infinitely large system.

Figure 8 shows the variation of π as a function of H for $\text{Re} = 100$. For $H \rightarrow 1$ the participation ratio approaches a value of $\pi_0 = 0.7$, which is the expected value for a Poiseuille flow between two parallel plates (see Section III of the Supplemental Material). By decreasing H , the participation ratio decreases monotonically indicating a stronger preferential channeling effect. Also shown in Fig. 8 is the participation ratio computed only in the $w/2$ -level surface, defined as the surface for which all points are at the vertical half distance between the lower and upper boundary of the crack. Compared to the bulk flow, the kinetic energy is distributed more homogeneously in this surface as the effect of the wall roughness is minimal. In this case, π also increases with the Hurst exponent, reflecting the formation of flow channels in fractures generated with low values of H .

IV. CONCLUSIONS

In summary, we have presented an extensive numerical study of single-phase flow through three-dimensional self-affine fracture joints. Our results show that the hydraulic resistance of the fracture to the flow G at low Reynolds numbers follows Darcy's law with a dependence on the Hurst exponent that can be explained in terms of a purely geometrical model for the channel tortuosity τ . For higher values of Re , at the onset of inertial effects in the flow, we find that nonlinear second- and third-order corrections to Darcy's law are approximately proportional to H . These results enable us to propose a universal curve to describe the variation of G with Re at laminar flow conditions

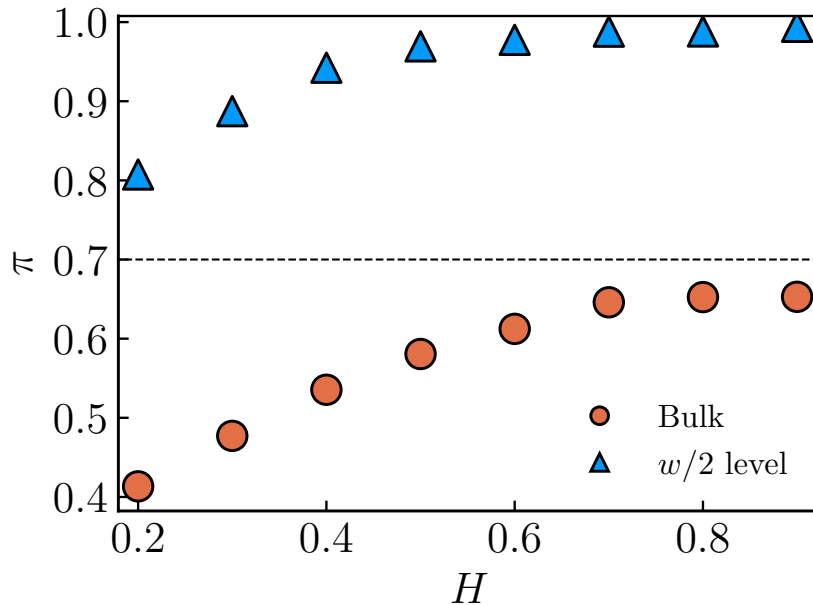


FIG. 8. Participation index π as a function of the Hurst exponent H . Red circles correspond to the bulk participation index and the blue triangles denote the participation index in the $w/2$ -level surface, obtained by translating the bottom surface of the channel by $w/2$ in the z -direction. The dashed horizontal line corresponds to $\pi = \pi_0$, namely, the value of participation for the flow at low Re between two parallel plates. The results were obtained by statistically averaging over five realizations.

and for any value of H . Finally, we find that preferred flow paths arise in the flow field, indicating that, even in three-dimensional fracture joints with no shear displacement between top and bottom surfaces, the effective fracture aperture field is heterogeneous.

ACKNOWLEDGMENTS

We thank the Brazilian agencies CNPq, CAPES and FUNCAP, also the National Institute of Science and Technology for Complex Systems and Petrobras for financial support.

-
- [1] M. Sahimi, “Flow phenomena in rocks: from continuum models to fractals, percolation, cellular automata, and simulated annealing,” *Rev. Mod. Phys.* **65**, 1393–1534 (1993).
 - [2] B. Berkowitz, “Characterizing flow and transport in fractured geological media: A review,” *Adv. Water Resour.* **25**, 861–884 (2002).
 - [3] M. Sahimi, *Flow and Transport in Porous Media and Fractured Rock: From Classical Methods to Modern Approaches* (Wiley-VCH Verlag GmbH & Co. KGaA, Weinheim, Germany, 2011).
 - [4] S. G. Osborn, A. Vengosh, N. R. Warner, and R. B. Jackson, “Methane contamination of drinking water accompanying gas-well drilling and hydraulic fracturing,” *Proc. Natl. Acad. Sci. U.S.A.* **108**, 8172–8176 (2011).
 - [5] L. Williams, P. Macnaghten, R. Davies, and S. Curtis, “Framing “fracking”: Exploring public perceptions of hydraulic fracturing in the United Kingdom,” *Public Underst. Sci.* **26**, 89–104 (2017).
 - [6] J.E. Warren and P.J. Root, “The Behavior of Naturally Fractured Reservoirs,” *Society of Petroleum Engineers Journal* **3**, 245–255 (1963).
 - [7] R. Liu, B. Li, Y. Jiang, and N. Huang, “Review: Mathematical expressions for estimating equivalent permeability of rock fracture networks,” *Hydrol. J.* **24**, 1623–1649 (2016).
 - [8] M. K. Hubbert and D. G. Willis, “Mechanics of Hydraulic Fracturing,” *Trans. Am. Inst. Min. Metall. Eng.* **210**, 153–163 (1957).
 - [9] J. L. Rubinstein and A. B. Mahani, “Myths and facts on wastewater injection, hydraulic fracturing, enhanced oil recovery, and induced seismicity,” *Seismol. Res. Lett.* **86**, 1060–1067 (2015).

- [10] S. Roux, J. Schmittbuhl, J. P. Vilotte, and A. Hansen, “Some Physical Properties of Self-Affine Rough Surfaces,” *Europhys. Lett.* **23**, 277 (1993).
- [11] L. Talon, H. Auradou, and A. Hansen, “Permeability of self-affine aperture fields,” *Phys. Rev. E* **82**, 46108 (2010).
- [12] L. Talon, H. Auradou, and A. Hansen, “Permeability estimates of self-affine fracture faults based on generalization of the bottleneck concept,” *Water Resour. Res.* **46**, W07601 (2010).
- [13] M. Wang, Y.-F. Chen, G.-W. Ma, J.-Q. Zhou, and C.-B. Zhou, “Influence of surface roughness on nonlinear flow behaviors in 3D self-affine rough fractures: Lattice Boltzmann simulations,” *Adv. Water Resour.* **96**, 373–388 (2016).
- [14] A. Bunde and S. Havlin, eds., *Fractals and Disordered Systems* (Springer Berlin Heidelberg, Berlin, Heidelberg, 1996).
- [15] E. Bouchaud, G. Lapasset, and J. Planès, “Fractal dimension of fractured surfaces: A universal value?” *Epl* **13**, 73–79 (1990).
- [16] K. J. Måløy, A. Hansen, E. L. Hinrichsen, and S. Roux, “Experimental measurements of the roughness of brittle cracks,” *Phys. Rev. Lett.* **68**, 213–215 (1992).
- [17] J. Schmittbuhl, S. Gentier, and S. Roux, “Field measurements of the roughness of fault surfaces,” *Geophys. Res. Lett.* **20**, 639–641 (1993).
- [18] B. L. Cox and J. S.Y. Wang, “Fractal Surfaces: Measurement and Applications in the Earth Sciences,” *Fractals* **01**, 87–115 (1993).
- [19] J. Schmittbuhl, F. Schmitt, and C. Scholz, “Scaling invariance of crack surfaces,” *J. Geophys. Res.* **100**, 5953–5973 (1995).
- [20] E. Bouchaud, “Scaling properties of cracks,” *J. Phys.: Condens. Matter* **9**, 4319 (1997).
- [21] A. P. Oron and B. Berkowitz, “Flow in rock fractures: The local cubic law assumption reexamined,” *Water Resour. Res.* **34**, 2811–2825 (1998).
- [22] N. E. Odling, “Natural fracture profiles, fractal dimension and joint roughness coefficients,” *Rock Mech. Rock Eng.* **27**, 135–153 (1994).
- [23] D. Amitrano and J. Schmittbuhl, “Fracture roughness and gouge distribution of a granite shear band,” *J. Geophys. Res. Solid Earth* **107**, 2375 (2002).
- [24] L. Ponsou, D. Bonamy, and E. Bouchaud, “Two-Dimensional Scaling Properties of Experimental Fracture Surfaces,” *Phys. Rev. Lett.* **96**, 35506 (2006).
- [25] T. Babadagli, X. Ren, and K. Develi, “Effects of fractal surface roughness and lithology on single and multiphase flow in a single fracture: An experimental investigation,” *Int. J. Multiph. Flow* **68**, 40–58 (2015).
- [26] M. Sahimi, “Long-range correlated percolation and flow and transport in heterogeneous porous media,” *J. Phys. I France* **4**, 1263–1268 (1994).
- [27] F. A. L. Dullien, *Porous media: fluid transport and pore structure* (Academic Press, San Diego, 1992).
- [28] G. Drazer and J. Koplik, “Permeability of self-affine rough fractures,” *Phys. Rev. E* **62**, 8076–8085 (2000).
- [29] E. Skjetne, A. Hansen, and J. S. Gudmundsson, “High-velocity flow in a rough fracture,” *J. Fluid Mech.* **383**, 1–28 (1999).
- [30] C. C. Mei and J.-L. Auriault, “The effect of weak inertia on flow through a porous medium,” *J. Fluid Mech.* **222**, 647–663 (1991).
- [31] J. C. Wodie and T. Levy, “Nonlinear Rectification of Darcy Law,” *Comptes Rendus L Acad. Des Sci. Ser. Ii* **312**, 157–161 (1991).
- [32] P. Forchheimer, “Wasserbewegung durch Boden,” *Z. Ver. Dtsch. Tsch. Ing.* **45**, 1782 (1901).
- [33] S. Briggs, B. W. Karney, and B. E. Sleep, “Numerical modeling of the effects of roughness on flow and eddy formation in fractures,” *J. Rock Mech. Geotech. Eng.* **9**, 105–115 (2017).
- [34] E. A. Oliveira, K. J. Schrenk, N. A. M. Araújo, H. J. Herrmann, and J. S. Andrade, “Optimal-path cracks in correlated and uncorrelated lattices,” *Phys. Rev. E* **83**, 046113 (2011).
- [35] P. A. Morais, E. A. Oliveira, N. A. M. Araújo, H. J. Herrmann, and J. S. Andrade, “Fractality of eroded coastlines of correlated landscapes,” *Phys. Rev. E* **84**, 16102 (2011).
- [36] B. B. Mandelbrot and J. W. van Ness, “Fractional Brownian Motions Fractional Noises and Applications,” *SIAM Rev.* **10**, 422 (1968).
- [37] M. F. Barnsley, R. L. Devaney, B. B. Mandelbrot, H.-O. Peitgen, D. Saupe, and R. F. Voss, *Leonardo*, edited by Heinz-Otto Peitgen and Dietmar Saupe, Vol. 22 (Springer New York, New York, NY, 1988) p. 455.
- [38] R. A. Earnshaw, ed., *Fundamental Algorithms for Computer Graphics* (Springer Berlin Heidelberg, 1991).
- [39] A. Hansen, J. Schmittbuhl, and G. G. Batrouni, “Distinguishing fractional and white noise in one and two dimensions,” *Phys. Rev. E* **63**, 62102 (2001).
- [40] H. G. Weller, G. Tabor, H. Jasak, and C. Fureby, “A tensorial approach to computational continuum mechanics using object-oriented techniques,” *Comput. Phys.* **12**, 620–631 (1998).
- [41] S. Whitaker, “The Forchheimer equation: A theoretical development,” *Transp. Porous Media* **25**, 27–61 (1996).
- [42] M. Sahini, *Applications of Percolation Theory* (CRC Press, 1994).
- [43] D. A. Edwards, M. Shapiro, P. Bar-Yoseph, and M. Shapira, “The influence of Reynolds number upon the apparent permeability of spatially periodic arrays of cylinders,” *Phys. Fluids A* **2**, 45–55 (1990).
- [44] J. S. Andrade, U. M. S. Costa, M. P. Almeida, H. A. Makse, and H. E. Stanley, “Inertial Effects on Fluid Flow through Disordered Porous Media,” *Phys. Rev. Lett.* **82**, 5249–5252 (1999).
- [45] R. J. Hill, D. L. Koch, and A. J. C. Ladd, “The first effects of fluid inertia on flows in ordered and random arrays of spheres,” *J. Fluid Mech.* **448**, 213–241 (2001).
- [46] Y. Chen, W. Liang, H. Lian, J. Yang, and V. P. Nguyen, “Experimental study on the effect of fracture geometric characteristics on the permeability in deformable rough-walled fractures,” *Int. J. Rock Mech. Min. Sci.* **98**, 121–140 (2017).
- [47] G. K. Batchelor, *An Introduction to Fluid Dynamics* (Cambridge University Press, 2000).

- [48] T. Ishibashi, N. Watanabe, N. Hirano, A. Okamoto, and N. Tsuchiya, “Beyond-laboratory-scale prediction for channeling flows through subsurface rock fractures with heterogeneous aperture distributions revealed by laboratory evaluation,” *J. Geophys. Res. Solid Earth* **120**, 106–124 (2015).
- [49] G. Drazer and J. Koplik, “Transport in rough self-affine fractures,” *Phys. Rev. E* **66**, 26303 (2002).
- [50] T. S. Lo and J. Koplik, “Channeling and stress during fluid and suspension flow in self-affine fractures,” *Phys. Rev. E* **89**, 23010 (2014).
- [51] N. Huang, Y. Jiang, R. Liu, B. Li, and Z. Zhang, “A Predictive Model Of Permeability For Fractal-Based Rough Rock Fractures During Shear,” *Fractals* **25**, 1750051 (2017).